Capabilities of Solmirus' Demonstration All Sky Visible Analyzer (D-ASIVA)

Date: December 4, 2008

Prepared for: Dr. Jacques Sebag
LSST Project

Prepared by: Dr. Dimitri Klebe
Solmirus Corporation

Introduction:

The Solmirus All Sky Infrared Visible Analyzer (ASIVA) is a commercially available multi-purpose visible and infrared sky imaging and analysis instrument designed to operate autonomously or as a component in an instrument cluster. Its utility ranges from astronomy and meteorology to military applications. Potential data products include the following:

- Cloud/No Cloud Reporting
- Cloud cover determination
- Photometric Quality Assessment
- Sky Opacity/Transmission determination
- Visible/IRcorrelation and integration
- Water vapor and Ozone determination
- Sky/Cloud temperature (brightness and color) measurements
- All-Sky (180 degree field-of-view) maps and analysis

To demonstrate ASIVA's capabilities and to refine data acquisition and analysis techniques, Solmirus has fabricated a demonstrational ASIVA unit (D-ASIVA). The D-ASIVA unit has just returned from a successful 2-month (11JUN2008 to 11AUG2008) deployment on Mauna Kea, HI. The instrument clearly demonstrated its ability to detect all clouds from cold, thin cirrus to clouds not visible on D-ASIVA's optical all-sky camera even when illuminated by the moon or at sunrise. Figures 1 and 2 below show some of the data acquired and analysis that was done during this field campaign.

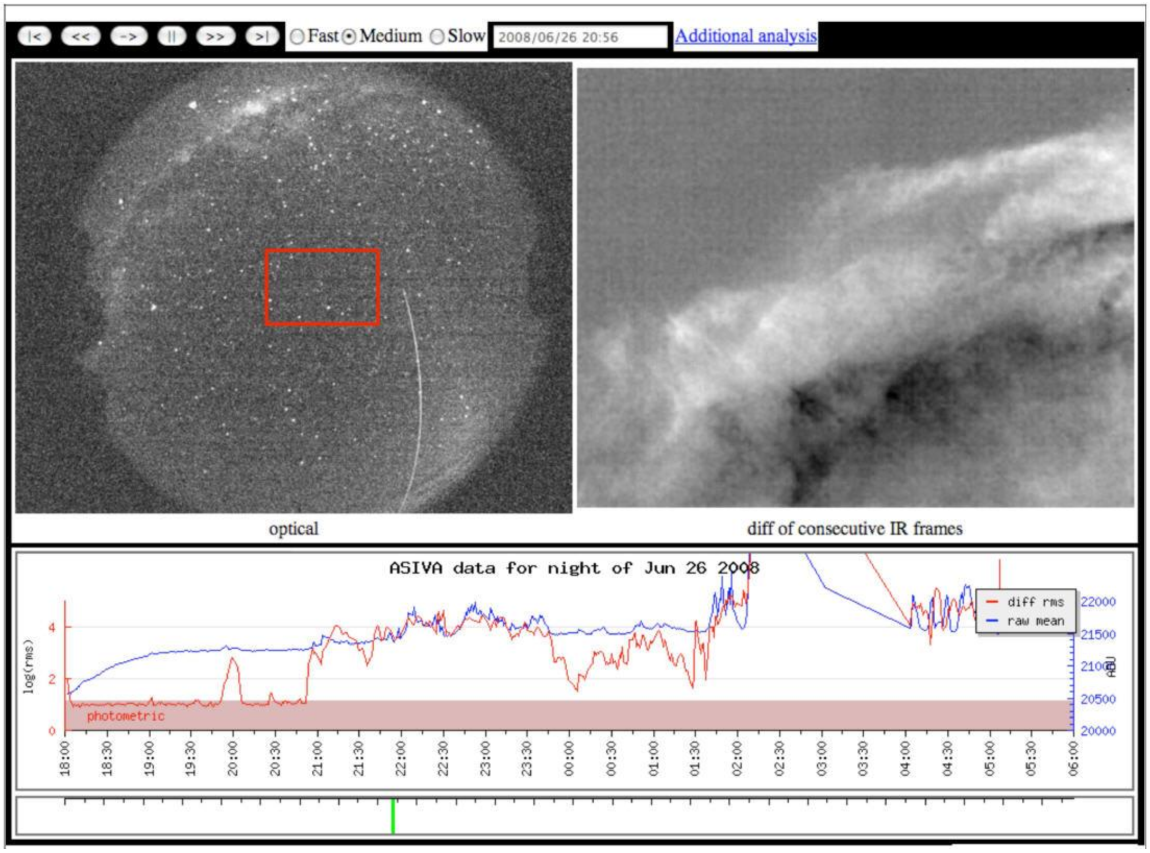

Figure 1: The CFHT (Canada France Hawaiian Telescope) Analysis Webpage showing both the D-ASIVA visible (left; FOV 180deg) and the mid-IR (right; FOV 38deg x 50deg) difference image. Just below the images the plot show the RMS (Root Mean Square) of the mid-IR difference frame in red and the blue line show the mean value of the raw data. When the RMS is within the red region, the sky is photometric. The green line in the lowest plot show where in the night's time sequence is being viewed. Also seen in the visible image is the KECK telescope AO (Adaptive Optics) laser guide star.

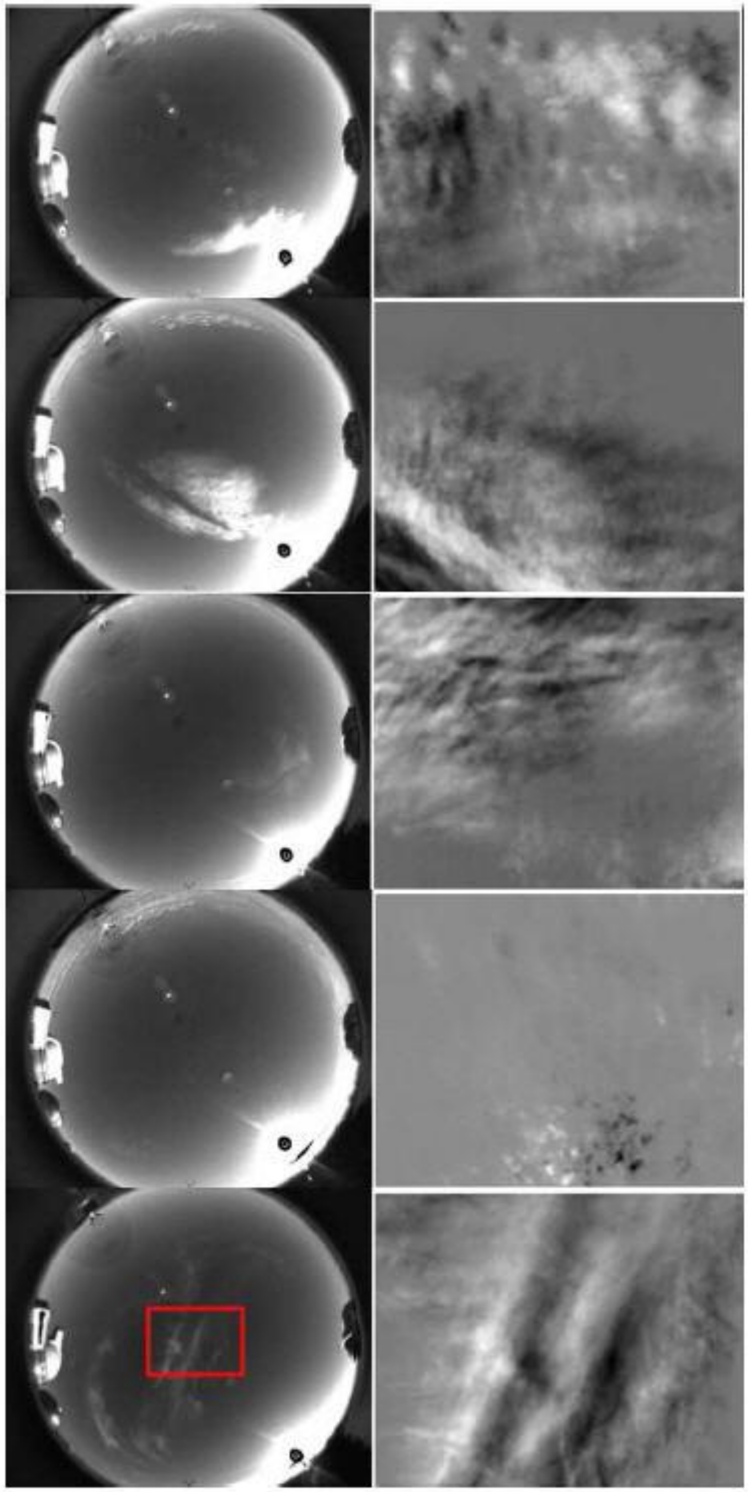

Figure 2: Images taken at sunrise with visible and mid-IR difference images taken at the same time. The red box in the bottom image is the field-of-view of the mid-IR image on the optical image. Note the significant amount of cloud structure seen in the mid-IR that is not apparent in the optical.

D-ASIVA's System Architecture:

A block diagram of the D-ASIVA instrument (as it is currently configured) and its primary functionality is shown below:

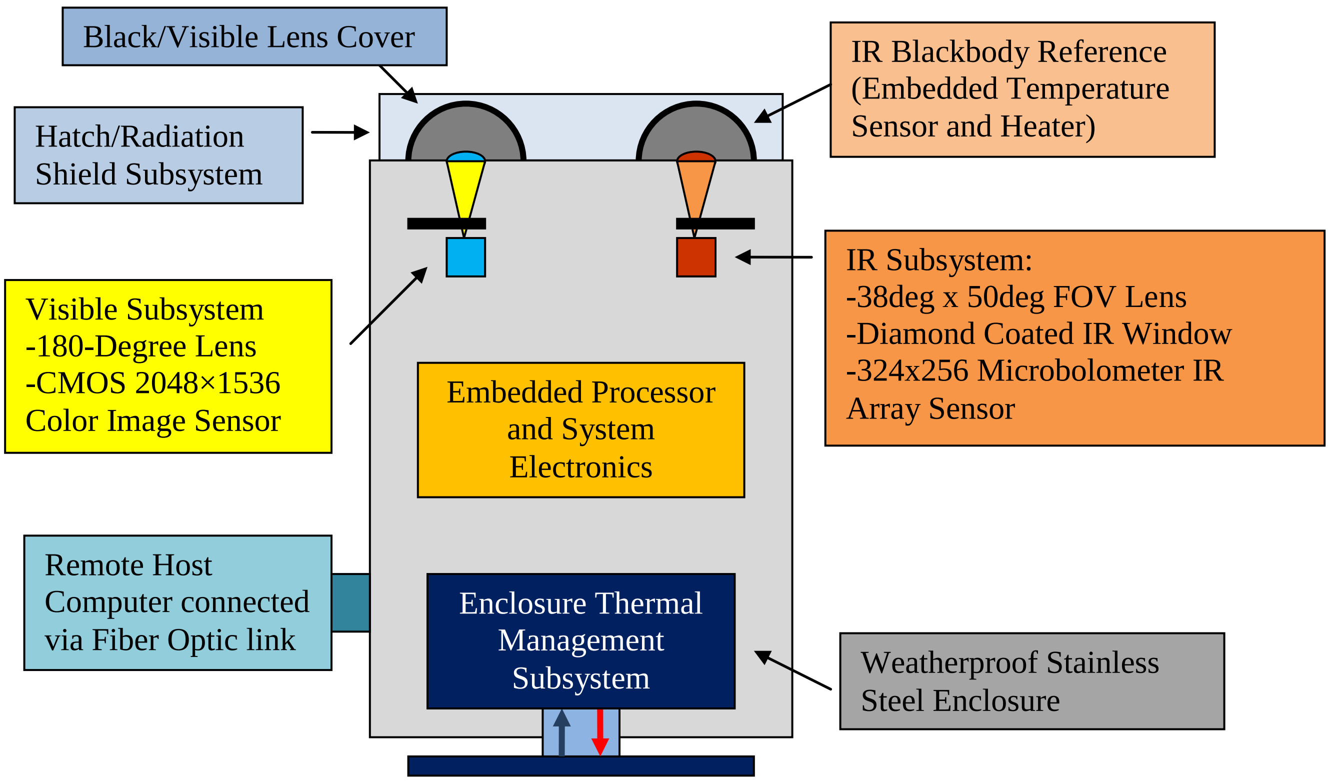

At the heart of the D-ASIVA instrument lays the infrared and visible imaging subsystems. The infrared subsystem includes a 324×256 uncooled microbolometer array sensitive to 8-14 micron radiation, an f/1.3 38degx50deg FOV lens, and a diamond coated window that allows the instrument's hatch to be open during inclement weather. In its current configuration the IR camera is pointed at the zenith but can be pointed as much as 45 degrees from zenith without changing the orientation of the enclosure. The D-ASIVA is currently not equipped with a filter wheel and is operated broad band with an effective bandpass from 8-13 microns. A six-position filter wheel for use with 1-inch filters will be added in the near future. The visible subsystem consists of a 2048×1536 CMOS color detector coupled with a 180-degree off-the-shelf lens. Images shown above from the HI field campaign demonstrates the camera's sensitivity in the g (green) band.

The brain of the ASIVA instrument is the embedded processor that communicates with and controls the imaging subsystems and other subsystems such as the hatch-motor, filter-wheel, temperature-meters, and weather-monitoring subsystems. Data (both raw and processed) is passed over a fiber optic link to the host computer where it can be archived and displayed. Operational control of the ASIVA instrument, additional image processing, and off-site control through the Internet is done via the host computer.

The D-ASIVA utilizes an innovative hatch mechanism that provides the following features:

- The blackbody reference remains in the same protected orientation (pointed downward) as the hatch mechanism is opened and closed.
- The hatch drive motor, position encoder, and limit switches are housed within the enclosure for better protection and durability.
- A temperature sensor is embedded in the IR blackbody reference for accurate in situ temperature measurements of the external environment.
- A heater element is embedded within the IR blackbody reference for accurate in situ temperature/flux calibration.
- The hatch mechanism provides a cover and calibration reference for both the IR and Visible subsystems.
- The IR blackbody and visible reference is covered by an insulated radiation shield allowing it to better track the ambient temperature as well as improves its performance in inclement weather.

An autonomous enclosure thermal management system (heating/cooling) is also located on-board the D-ASIVA unit to maintain the proper internal operating temperature for the D-ASIVA components. This system is designed to handle wide swings in external temperature and is useful for the longevity of the instrument and its hardware. Regulation of internal temperature also aids in providing good absolute flux calibration. The D-ASIVA as it is currently configured is shown below.

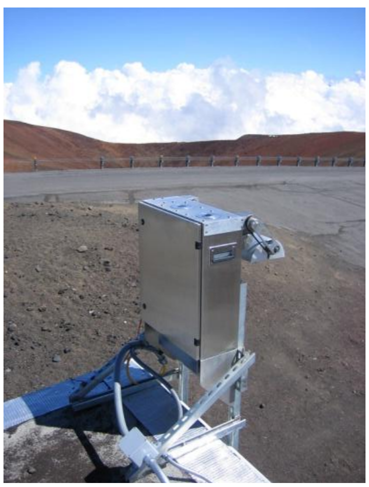

D-ASIVA on Mauna Kea, HI

D-ASIVA in Colorado Springs, CO

D-ASVIA Data Products and Analysis:

The D-ASIVA's primary function is to provide radiometrically-calibrated imagery in the mid-infrared (IR) atmospheric window. The D-ASIVA is currently configured to operate in a broad band (8-13 micron) mode. The following figures show clear sky atmospheric transmission in this spectral interval.

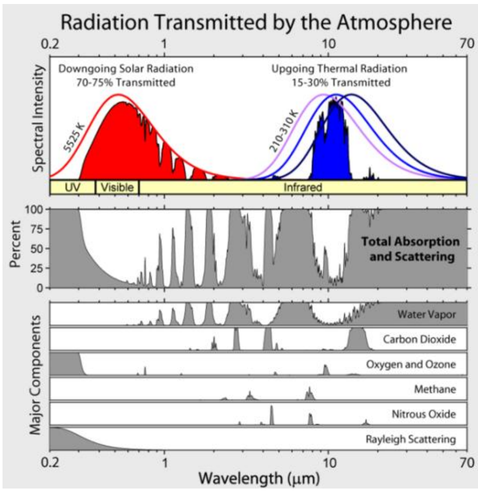

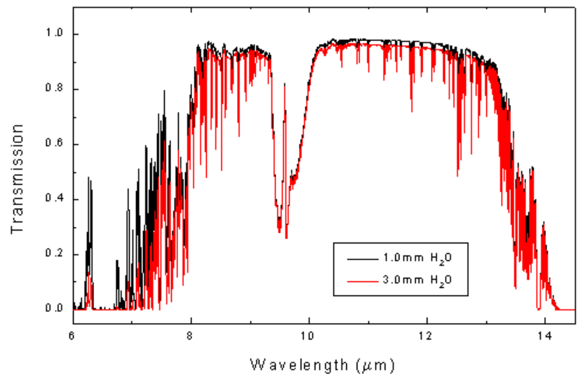

Absorption is dominated by water vapor at wavelengths less than 8 microns, by carbon dioxide at wavelengths greater than 13 microns, and by ozone near 9.5 microns. Water vapor lines, however, are seen strewn throughout this spectral interval but are least prevalent in the 10.2-12.2 micron region. Solmirus will be procuring a custom 10.2-12.2 micron filter for the Hawaii ASIVA system. Several filters will be ordered and a filter will be made available for the D-ASIVA. This filter is highly recommended in detecting clouds in humid environments.

Clouds are essentially gray bodies and are easily detected against the background of the highly transmitting sky. For flux calibrated images, Solmirus utilizes the following radiometric calibration procedure for its ASIVA instruments. The instrumental gain $D(\lambda)$ for a specific filter is calculated using the following equation.

$$D_\lambda = \frac{I_\lambda}{\epsilon_\lambda \cdot BB_\lambda(T)} \quad \left\{\frac{Counts}{Watts/m^2/sr}\right\}$$

Where:

$$I_\lambda = Instrumental\ Counts\ Measured\ for\ a\ specific\ filter$$

$$\epsilon_\lambda = Emissivity\ of\ the\ Blackbody\ Reference$$

And

$$BB_\lambda(T) = \int \frac{1.1911 \times 10^8 \cdot \lambda^{-5}}{e^{14{,}388/\lambda T} - 1} d\lambda \quad \{Watts/m^2/sr\}$$

Note: The blackbody equation $BB_\lambda(T)$ above assumes a wavelength λ given in units of microns and is integrated over the filter's bandpass for a particular temperature T given in

Kelvin. The emissivity (ϵ_λ) of the blackbody depends on the coating used for the calibration reference and is assumed to be constant over the filter bandpass. The D-ASIVA calibration reference uses a flat black paint with an assumed emissivity of 0.95. Higher emissivity coatings (with known emissivity) are available on production models. One of these coatings will be sought for the D-ASIVA unit when the next high-emissivity coating run is made.

To account for instrumental offsets, D_λ is calculated by plotting I_λ vs. $BB_\lambda(T)$ for a range of temperatures T and determining the best straight line fit to the data. This analysis assumes that the infrared microbolometer used in the ASIVA has a linear response. Preliminary calibration runs indicate the microbolometer to have a linear response.

Blackbody reference and calibration data is collected using D-ASIVA's hatch cover mechanism. The hatch containing the blackbody reference is used to periodically cover the infrared window/lens. A temperature sensor is embedded in the calibration reference and the blackbody temperature is written into the FITS file header when acquiring reference and calibration data. A heater is built into the calibration reference so that I_λ for a range of temperatures can be acquired in situ and in a short period of time to substantially reduce possible systematic errors caused by temperature changes in system components (lens, sensor, etc.) during the calibration procedure. The calibration procedure is run by simply executing the calibration command on the D-ASIVA host computer. When executed, the blackbody reference is heated to ~60 °C and allowed to cool. The hatch is closed to acquire data each time the blackbody reference has cooled another 5 °C until it has cooled to 5 °C above ambient. When data is not being acquired, the hatch is left open to avoid heating the IR window/lens. The data is then analyzed as described above and a gain image is written to disk to be used in calibrating sky images thereafter. This calibration procedure need not be done often. It is required to maintain good absolute calibration as the instrument weathers.

Flux-calibrated $F_{\lambda_{Sky}}$ sky images for given filters are then determined using the following relation:

$$F_{\lambda_{Sky}} = \frac{I_{\lambda_{Sky}} - I_{\lambda_{Ref}}}{D_\lambda} + BB_\lambda\left(T_{Ref}\right)$$

Where $BB_\lambda\left(T_{Ref}\right)$ is the integrated blackbody flux derived from the temperature of a reference blackbody (T_{Ref}) acquired at approximately the same time as the sky observation. For the HI field campaign, a reference was acquired at the top of the hour and an IR image was acquired once a minute. During twilight conditions when the temperature is changing more rapidly, reference flats should be taken more frequently to maintain good calibration. The hatch can be opened and closed in a few seconds so reference flats can be taken every minute if needed.

The brightness temperature of the sky (T_{Sky}) can be calculated by setting the flux ($F_{\lambda_{Sky}}$) equal to a blackbody of a given temperature that would produce this flux. Solving for T_{Sky} we have:

$$T_{Sky} = \frac{14{,}388}{ln\left[\dfrac{1.1911 \times 10^8 \cdot \lambda^{-5} \cdot \Delta\lambda}{BB_\lambda(T_{Ref}) + \dfrac{I_{\lambda_{Sky}} - I_{\lambda_{Ref}}}{D_\lambda}} + 1\right]}$$

Where in this case λ is the central wavelength of the filter and $\Delta\lambda$ is its bandpass in microns. For clouds that are optically thick, the brightness temperature essentially yields the temperature of the cloud.

Often a more revealing metric is the temperature difference between the sky and the ground given by:

$$T_{Diff} = T_{Sky} - T_{Ref}$$

High temperature differences indicate clear sky condition whereas low temperature differences reflect opaque low lying clouds.

Another revealing metric is simply to map the normalized flux ratio given by:

$$F_{\lambda_{Sky}} \Big/ BB_\lambda(T_{Ref}) = \frac{I_{\lambda_{Sky}} - I_{\lambda_{Ref}}}{D_\lambda} \Big/ BB_\lambda(T_{Ref}) \; + \; 1$$

This measurement is an approximate measure of the emissivity of the sky and is an exact measure in cases where the sky temperature is the same as the reference temperature on the ground. Clear skies will produce flux ratios near 0.0 and cloudy skies will produce flux ratios near 1.0.

The data products discussed above are available on the D-ASIVA. Sky images are currently stored as a 3-dimensional FITS image 324 x 256 pixels by 16 images deep. Each image in the 3-D FITS image represents ~0.5 seconds exposure acquired by co-adding 16 1/30th second frames. The 3-D FITS image can therefore be co-added to provide a single ~8 second exposure. This data collection scheme worked well for the HI field campaign but can be easily modified if necessary.

The D-ASIVA currently achieves a Noise Equivalent Power (NEP) of 0.016 W/m^2/sr for a single 0.5 second image. NEP is determined by differencing consecutive images and calculating its RMS fluctuations. Similar results are obtained by calculating the RMS fluctuations for each pixel using the 16 individual values stored for that pixel in the 3-D image file. The NEP specification equates to a Noise Equivalent Temperature Difference (NETD, computed at 300 K) of 20 mK which compares very nicely with the camera manufacturer's quoted NETD specification for a single 1/30th second frame of 85 mK. At T = 273 K, one can also translate the NEP specification to a noise equivalent optical depth of 0.0005. This means that one should be able to detect optical depth (and therefore sky emissivity/transmission) variations at the 0.5% level with a signal to noise ratio of 10. A factor of four improvement in S/N ratio is obtained by co-adding the 16 images stored in the 3-D FITS file. We anticipate a reduction in S/N ratio of ~5 when utilizing narrower (~1-micron) bandpass filters. The following images represent a sample of radiometrically-calibrated images taken in Colorado Springs before the D-ASIVA instrument was shipped to HI. Flux values are listed in W/m^2/sr and for reference $BB_{8-13\mu m}(300)$ = ~50 W/m^2/sr and $BB_{8-13\mu m}(273)$ =~30 W/m^2/sr.

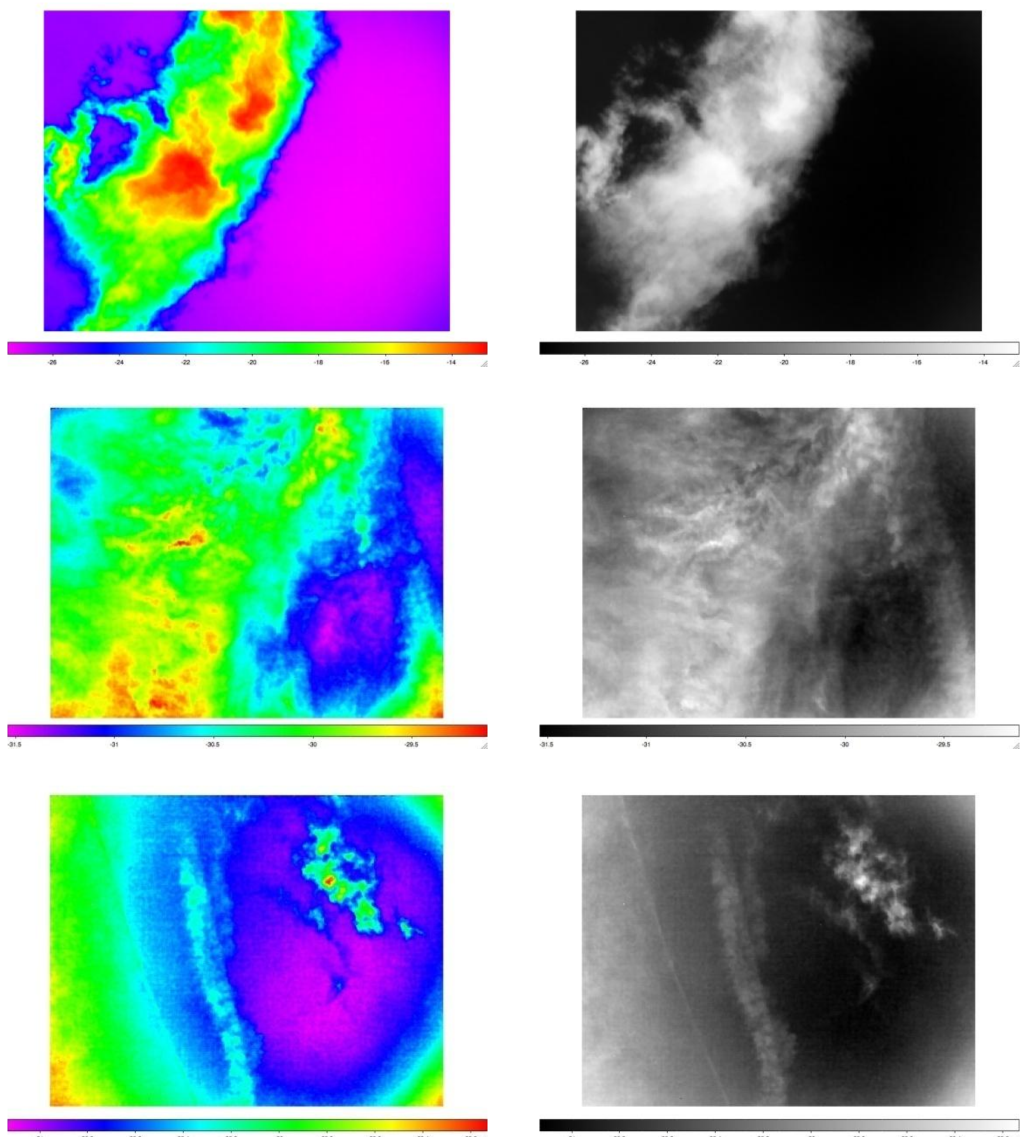

The radiometric calibration procedure described above does provide an absolute measure of the flux within a given filter's bandpass. However, the accuracy of this result has not been quantified. The most straightforward method would be to build a high-emissivity calibration source (utilizing the same high-emissivity coating discussed above) that can be placed in the field of view of the instrument whereupon its accuracy can be measured directly. This technique is under investigation and primarily depends on funding.

Providing absolute transmission data in a given bandpass requires knowledge of the mean temperature of the radiating atmosphere/cloud. With a single bandpass system, as D-ASIVA is currently configured, there is no way to attain this information without a priori knowledge of the atmosphere. A simple method is to use a standard lapse rate for the site location and to infer the sky/cloud temperature from that taken on the ground. A more accurate measure would be to use an independent measure of the lapse rate taken by other means. A more sophisticated approach would be to compute the color temperature inferred by the flux ratio in two different filters. The calibration procedure for this technique is discussed below.

Instrumental gain ratios D_{λ_1/λ_2} between filters can be calculated using the following equation using an ensemble of blackbody reference data with known temperature.

$$D_{\lambda_1/\lambda_2} = \frac{I_{\lambda_1}/I_{\lambda_2}}{BB_{\lambda_1}(T)/BB_{\lambda_2}(T)}$$

Where the following simplified form of the blackbody equation is used.

$$BB_\lambda(T) = \frac{1.1911 \times 10^8 \cdot \lambda^{-5}}{e^{14,388/\lambda T} - 1} \quad \{Watts/m^2/\mu m/sr\}$$

Color temperature can be determined from the following equation:

$$\frac{BB_{\lambda_1}(T_{Color})}{BB_{\lambda_2}(T_{Color})} = \frac{I_{\lambda_1}/I_{\lambda_2}}{D_{\lambda_1/\lambda_2}} = (\lambda_2/\lambda_1)^5 \times \left(\frac{e^{14,388/\lambda_2 T_{Color}} - 1}{e^{14,388/\lambda_1 T_{Color}} - 1}\right)$$

The value T_{Color} cannot be solved directly but it can be determined iteratively or through a lookup table. The following table shows the blackbody flux ratio sensitivity to color temperature for wavelengths centered at $\lambda_1 = 8.0$ and $\lambda_2 = 12.0$ microns respectively.

$T_{Color}(K)$	200	210	220	230	240	250	260	270	280	290	300
$\frac{BB_{8.0}(T_{Color})}{BB_{12.0}(T_{Color})}$	.38	.44	.50	.56	.62	.69	.75	.82	.88	.95	1.01

As one can see the blackbody flux ratio is very sensitive to color temperature. The color temperature is a much better indicator of cloud temperatures especially in optically thin conditions assuming the optical depth is constant across the wavelength interval. The color temperature provides a good measure of the mean temperature of the emitting sky/cloud and as discussed above can be used to provide a much more accurate measure of the sky's/cloud's optical depth.

The D-ASIVA is currently configured to implement the following cloud detection procedures. The motivation for collecting 16 consecutive 0.5 second images was to allow more flexibility in developing cloud detection algorithms. In what we believe is the most promising technique, an RMS (Root Mean Square) map is created by calculating the RMS value for each pixel across the 16 images stored in the 3-D FITS file. The following RMS images were generated using this technique.

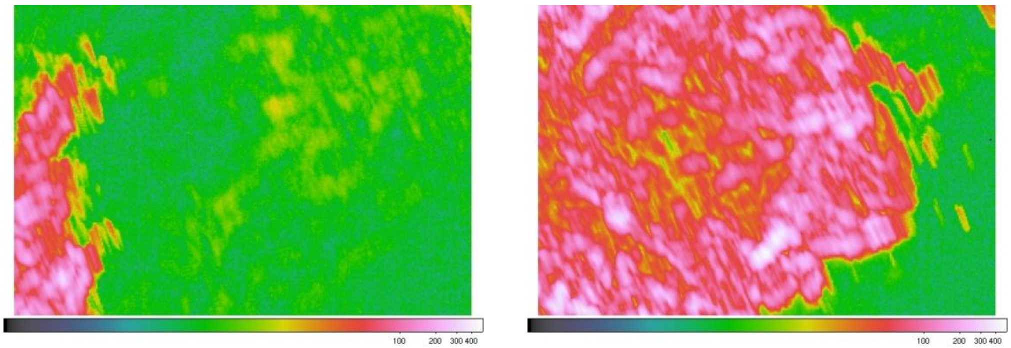

These images are displayed using a logarithmic scale and represent the RMS fluctuation for each pixel in instrument counts. The blurring seen in the images is due to cloud motions over the 8-second interval used to create this data set. The calibrated temperature maps for these two images are shown below where temperatures are given in Kelvin relative to the ground temperature.

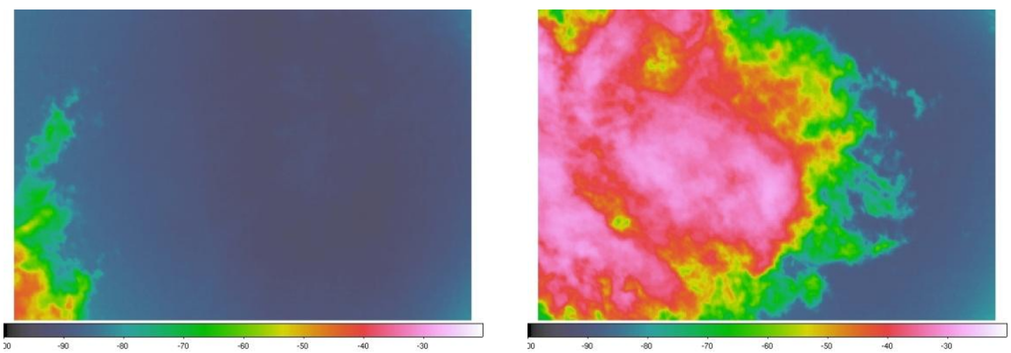

Note how the RMS technique readily identifies cloud structure in the left panel that is not seen easily in the temperature calibrated map. In producing a cloud/no cloud mask using the RMS data, one simply needs to establish an RMS threshold above which, the pixel is considered to be a cloud. One should also note in the right panel that RMS values are diminished in the central region of the cloud where it is brightest. This suggests that RMS values alone may not be able to properly determine the cloud/no cloud status of a particular pixel. To combat this, we suggest a multiple tier algorithm to ultimately determine the cloud/no cloud status of a given pixel. As indicated above, one could establish a brightness temperature/flux threshold that could also determine cloud/no cloud status. In the above example, this would eliminate the issues encountered in the central region of the solid optically thick cloud.

Another technique in cloud/no cloud determination that has been explored is examining the RMS variations associated with a difference image created from the data. For the above data set, a difference image is created that represented the difference between the sum of images 1,3,5,…,15 and the sum of images 2,4,6,…16 collected for the 3-D FITS files. These difference images are then further processed by replacing each pixel by the RMS variation of a 9x9 box centered on that pixel. Results of that analysis are shown below.

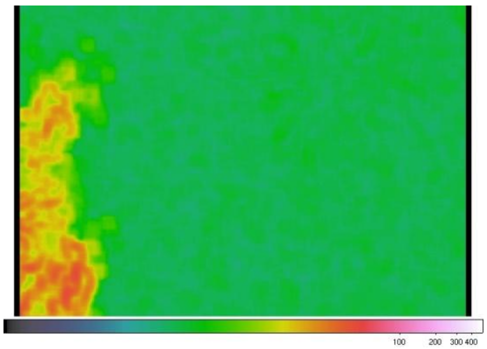

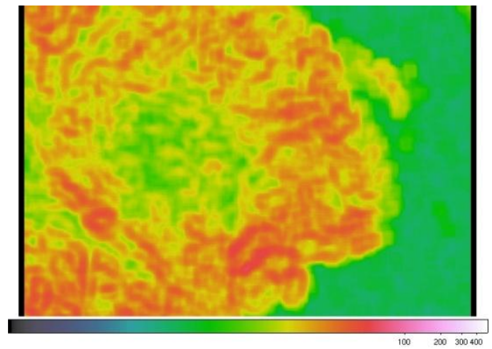

The reduced contrast of these images suggests that this RMS difference technique is not as powerful as the RMS technique previously discussed. We, however, do not want to dismiss this technique as it still may prove useful. Both RMS techniques require cloud motion over the observation period to detect the presence of cloud structure. The RMS difference technique can be implemented more easily over longer stretches of time. As shown for the HI field campaign data, difference maps were created from each successive image taken at one minute intervals and proved to be a reliable metric in determining the presence of clouds.